# Effects and Opportunities of Seasonally Reversing Geothermal Flow Direction

AESB3400 Bachelor End Project

Author:
Lars Voorneveld
5842638

Supervised by:
Dr. A. (Alexandros) Daniilidis
Prof. Dr. P.J. (Phil) Vardon

Department of Geoscience and Engineering
Delft University of Technology

July 7th, 2025

## Acknowledgements

I would like to thank my supervisors Dr. A. Daniilidis and Prof. Dr. P.J. Vardon for their support and guidance during this bachelor thesis. The weekly meetings were very helpful to ensure that everything was on track to finish in the limited time available. Also outside the weekly meetings, their offices were always open to stop by for questions and advice. Furthermore, I would like to thank Yuan Chen for providing me the data from his numerical simulation of the Delft geothermal production temperatures. This data was very helpful to verify the analytical model.

# Abstract

Heating and cooling accounts for nearly half of the total energy consumption in the European Union, making geothermal systems a vital component for the energy transition. However, their operational lifetime is limited. Injected cold water forms a cold thermal front that spreads outwards. When this front reaches the production well, thermal breakthrough occurs and production temperatures drop. This report investigates whether seasonally reversing the flow direction by injecting hot water during periods of low heat demand can extend the reservoir's lifetime or allow for reduced well spacing. This is important because it can optimize the use of geothermal systems in the future.

To do this, annual energy demand was studied to find when heat demand is low. The available solar power in this period was then calculated for three different scenario's to determine what reversed flow rate can be delivered. After establishing an analytical model and baseline simulation of the Delft geothermal reservoir, the three scenario's were tested and the new breakthrough times computed. The effects of reservoir thickness and well-spacing were then studied.

It was found that with the solar power currently available on the TU Delft campus, the lifetime of the geothermal reservoir can be extended by 7 years from the original 21 years. With a limited expansion of solar power on campus, this extension could be 11 years and if the system is run at maximum capacity, 21 years is possible. It was found that if the lifetime were to be kept constant, the well spacing could be reduced from the original 1100 metres down to between 934.8 and 789.2 metres depending on the scenario.

It was concluded that seasonally reversing the flow direction offers several opportunities to optimize geothermal systems. Either by extending the lifetime of the geothermal system or by allowing closer well spacing to minimize costs whilst keeping a reasonable reservoir lifetime.

# Contents

# 1 Introduction

Heating and cooling of houses and other civil infrastructure requires a large amount of energy annually. As of 2022, the energy required for heating and cooling makes up about half of the total energy consumption in the European Union. In many countries, this energy is still largely provided by non-renewable sources. As can be seen in Figure 1 below, in 2022 only 25% of the energy required for heating in the EU was from renewable sources, with great variation between countries (Eurostat, 2024).

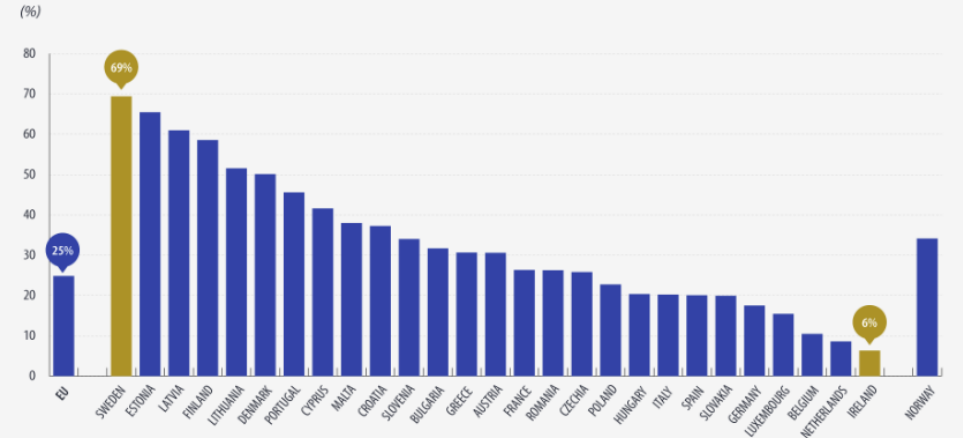


Figure 1: Share of renewable energy used for heating in the EU, (Eurostat, 2024)

In order to achieve the set climate targets, it's essential that the share of renewable energy in heating and cooling increases. Geothermal energy is one of the options to provide heating and cooling in the future. In Figure 2, a simple geothermal doublet system can be seen. A geothermal doublet setup consists of a production well and an injection well that are drilled to a porous reservoir, typically at depths of 1-3 kilometres. Hot reservoir water is extracted through the production well. This hot water is used in a heat exchanger to supply heat for district heating systems. The cold water is then re-injected in the original reservoir through the injection well.

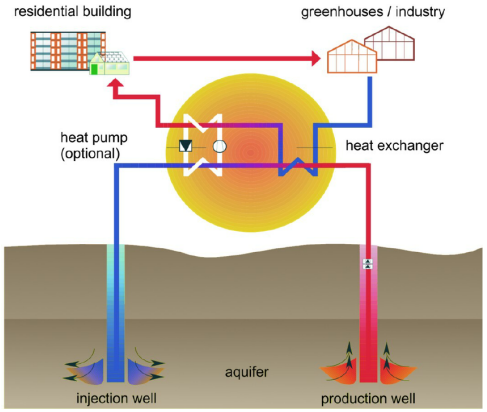


Figure 2: Simple geothermal doublet (Agemar, Weber & Schulz, 2014)

Despite being a renewable energy source, extracting warm water and re-injecting cold water means that energy is taken out of the system and thus the lifetime of geothermal setups is not unlimited. This is described in Fadel, Reinecker, Bruss, & Moeck, (2022), where it's mentioned that one of the main characteristic features of re-injection is that it creates a zone of cooled water around the injection well, which will grow with time. Eventually, the cold water front will reach the production well. When this thermal front reaches the production well, thermal breakthrough occurs and production temperatures drop. To supply heat for a reasonable amount of time, the wells are positioned a minimum distance from each other. Heat demand is not constant throughout the year. During summer months, demand is generally much lower. Temporarily reversing the flow direction in the geothermal doublet in this period could delay the advance of the thermal front. For this process, cold water is extracted and heated to reservoir temperatures at the surface using solar power in the summer months. This water is then injected into

the hot well to partly reverse the cold thermal front and extend the lifetime of the geothermal reservoir. Slowing down the advance of the cold thermal front could also allow for closer well spacing without reducing reservoir lifetime.

The goal of this report is to analyze the effects of seasonally reversing the flow direction in geothermal reservoirs and to see if, by doing this, the lifetime can be extended or the well spacing reduced. This leads to the main research question:

> *Can seasonal flow reversal be used to extend the operational lifetime of geothermal systems and enable reduced well spacing without compromising performance?*

To answer this main question, the report aims to answer the following sub-questions.

1. Which months are suitable for reversing geothermal flow direction and how much solar power is available during this time?
2. How much geothermal fluid can be reheated to reservoir temperature using this energy?
3. What is the effect of seasonal hot water injection on cold front progression and thermal breakthrough time?
4. How do reservoir properties such as thickness and well spacing change the effect of flow reversal?
5. Does flow reversal allow for closer well spacing whilst maintaining reservoir lifetime?

The report is structured as follows: first, background information and physical principles will be explained that are required to understand geothermal reservoirs and the flow and heat transport through porous media. After that, the methods used in the research will be explained. The results will then be presented and any uncertainties and limitations will be discussed before finally drawing a conclusion.

# 2 Background and physical principles

## 2.1 Geothermal reservoirs

Geothermal reservoirs are porous layers in the subsurface that are saturated with hot water. This hot water can be extracted and used for heating or generating electricity. After this, the cold water is re-injected in the reservoir. There are several crucial parameters that define a geothermal reservoir. The first one being porosity:

$$\phi = \frac{V_p}{V_b} \tag{1}$$

Where $V_p$ is the volume of pore space in the rock and $V_b$ is the bulk volume. The greater the porosity, the more pore space available for hot water.

Permeability is another important parameter. Permeability expresses how easy a fluid can flow through the porous medium. For easy extraction, high permeability is required.

For the temperature of the geothermal reservoir, the local temperature gradient is important. The temperature gradient is defined as

$$G = \frac{dT}{dZ} \tag{2}$$

Where dT is the change in temperature and dZ is the change in depth. On average, Earth's temperature gradient is 20 degrees per kilometer but this is often higher in places with geothermal systems (Nurmi & Oy, 2021).

To assess the quality of a geothermal reservoir, the amount of thermal energy stored in the reservoir has to be determined. This can be done using the equation below.

$$E = V \cdot [(1-\phi) \cdot \rho_r c_r + \phi \cdot \rho_f c_f] \cdot (T_r - Ti) \tag{3}$$

Where $E$ is the total thermal energy, $V$ is the reservoir bulk volume, $\phi$ is the porosity, $\rho_r$ and $\rho_f$ are the densities of the rock and fluid respectively, $c_r$ and $c_f$ are the specific heat capacities of the rock and fluid respectively, $T_r$ is the temperature of the reservoir and $T_i$ is the temperature of the re-injected water.

## 2.2 Flow and heat transport in porous media

One of the governing equations for flow in porous media is Darcy's law. For an incompressible fluid, Darcy's law is expressed as follows:

$$\overrightarrow{u} = -\frac{k}{\mu} \cdot \bigtriangledown P \tag{4}$$

Here, $\overrightarrow{u}$ is the darcy velocity, $k$ is permeability, $\mu$ is the fluid viscosity and $P$ is the pressure.

One of the limitations is that Darcy's law assumes laminar flow. Whether flow is considered laminar or non-laminar is determined by the Reynolds number. It's generally assumed that flow is laminar (and thus Darcy's law holds) for values below an upper limit for Re between 1-10 (Wang, Li, Zhao, Chen Nan-xiang, & Xu, 2019). Reynolds number is computed as shown in equation 5 below.

$$Re = \frac{\rho d_0 u}{\mu} \tag{5}$$

where $\rho$ is the fluid density, $d_0$ is the diameter of the grains in the reservoir, $u$ is the darcy velocity and $\mu$ is the dynamic viscosity of the fluid.

Another critical concept in modeling subsurface flow is the conservation of mass. This ensures that no mass is destroyed or created. The equation in it's basic form is shown below.

$$\frac{\partial}{\partial t}(\phi \rho_f) + \bigtriangledown \cdot (\rho_f \vec{u}) = 0 \tag{6}$$

where $\phi$ is porosity, $\rho_f$ is the fluid density and $\vec{u}$ is the darcy velocity.

When using an incompressible fluid (such as water), the density of the fluid $\rho_f$ and porosity $\phi$ are constant, thus $\frac{\partial}{\partial t}(\phi\rho_f) = 0$ and the equation simplifies to

$$\bigtriangledown \cdot \vec{u} = 0 \tag{7}$$

In geothermal reservoirs, this equation ensures that the fluid entering the reservoir equals the fluid being extracted from the reservoir.

When looking at heat transport in porous media, this mainly occurs through three mechanisms. The first one being conduction. In conduction, thermal energy is conducted through molecular interaction. It is described by Fourier's law:

$$\overrightarrow{q}_c = -\lambda_{eff}\nabla T \tag{8}$$

where $q_c$ is the conductive heat flux, $\lambda_{eff}$ is the effective thermal conductivity and $\nabla T$ is the temperature gradient.

The second mechanism is advection. In advection, heat is transported with the flowing fluid. The equation for advection is:

$$\overrightarrow{q}_a = \rho_f c_f \overrightarrow{u} T \tag{9}$$

where $q_a$ is the advective heat flux, $\rho_f$ is the density of the fluid, $c_f$ is the specific heat capacity of the fluid, $\overrightarrow{u}$ is the darcy velocity and T is the temperature.

The last mechanism is dispersion. Dispersion is caused by heterogeneity in a reservoir. This heterogeneity causes variations in flow paths at microscopic scale. This dispersion can cause earlier thermal breakthrough to occur than would be expected based on pure advection models because part of the injected fluid moves "ahead" of the front.

## 2.3 Lifetime of geothermal systems

In geothermal reservoirs, the lifetime is determined by when thermal breakthrough occurs. During operation, hot water is extracted from the reservoir and cold water is injected back into the reservoir through the cold well. This forms a cold thermal front that propagates through the porous medium towards the hot production well. When this cold thermal front reaches the production well, thermal breakthrough occurs and the production temperatures drop.

In porous media, the movement of the thermal front is determined by the conservation of energy. The temperature field evolves according to the following equation, which consists of the equations also mentioned above:

$$(\rho c)_{eff}\frac{\partial T}{\partial t} + \rho_f c_f \overrightarrow{u} \cdot \nabla T = \nabla \cdot (\lambda_{eff} \cdot \nabla T) \tag{10}$$

This equation takes into account the stored heat, advection and conduction.

To calculate thermal breakthrough time, one cannot simply use the Darcy velocity as this velocity gives the volumetric flow per unit cross-sectional area. To calculate the velocity of the fluid through the pores, one can use the following equation:

$$v_p = \frac{u_d}{\phi} \tag{11}$$

where $v_p$ is the pore velocity, $u_d$ is the darcy velocity and $\phi$ is the porosity.

From this, the velocity of the thermal front can be calculated using:

$$v_T = \frac{v_p}{1 + \frac{(1-\phi)\rho_r c_r}{\phi\rho_f c_f}} \tag{12}$$

where $v_T$ is the velocity of the thermal front, $v_p$ is the pore velocity, $\phi$ is the porosity, $\rho_r$ and $\rho_f$ are the densities of the rock and fluid respectively and $c_r$ and $c_f$ are the specific heat capacities of the rock and fluid respectively.

In simple linear flow, the thermal breakthrough time can then be computed as follows:

$$t_{breakthrough} = \frac{L}{v_T} \tag{13}$$

where $t_{breakthrough}$ is the time to thermal breakthrough, $L$ is the horizontal distance between the wells and $v_T$ is the velocity of the thermal front.

### 2.4 Reversing geothermal flow direction

In summer, energy demand -especially for heating purposes- is much lower than in winter. Reversing the direction of flow during summer would mean that cold water is extracted through the cold well, heated above the surface and then injected through the hot well. What this should do is partially reverse the advance of the thermal front, thus extending the time before the thermal front reaches the production well.

## 3 Methodology

This section aims to describe the methods and models used to answer the research questions. The section first aims to analyse the heat/energy demand to identify when reversed flow is possible. After that, the available solar power in this period will be calculated and three different scenario's will be presented. To perform the simulations, an analytical baseline model for thermal breakthrough will be set up to simulate the advance of the thermal front over time. After a sensitivity analysis for this model, it will be matched to the results from an established numerical model to determine the properties of our equivalent Delft reservoir. With the available solar power and the reservoir properties from the baseline simulation, the reversed flow rates will be calculated. The model will then be adjusted to periodically reverse the flow direction and re-simulate the position of the thermal front over time. With these results, the effects of thickness and well-spacing can be further analysed. A schematic flowchart of the methodology can be seen in Figure 3 below.

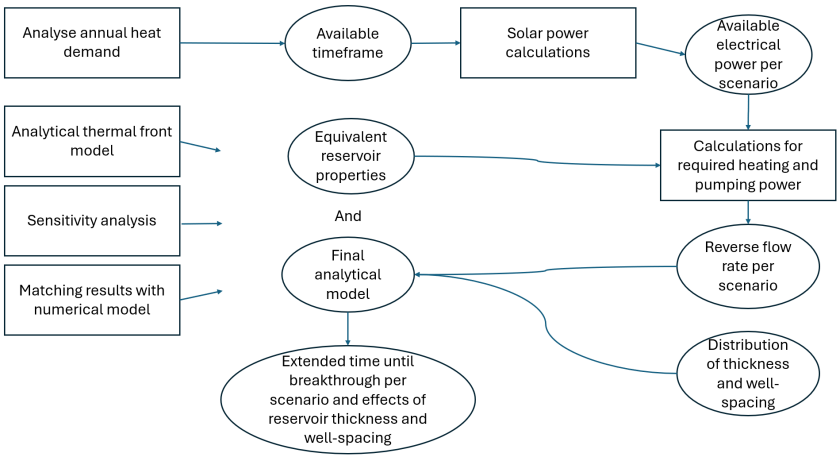


Figure 3: Methodology flowchart

### 3.1 Heat and energy demand

The first important step in this research is to understand how heat and energy demand vary over the year. The goal of this section is to identify the months of the year with low heat demand and a surplus of energy that are suitable to reverse the flow direction of the geothermal system and re-inject hot water into the reservoir.

To achieve this, average outside temperature data from the KNMI for a period of 14 years was obtained to plot the average monthly temperatures. Assuming that generally, heating systems are switched off when outside temperatures reach averages of around 14 degrees Celsius, this gives an indication of the

time-frame for reversing the flow direction. Literature research on ATES-systems in the Delft area was also used to visualize the energy demand. From this data, the yearly time frame available for reversed flow is determined.

## 3.2 Energy calculations

When reversing the flow direction. Power is required to heat the water. Several options for this were considered, including solar power combined with a heat exchanger, thermal solar collectors and direct electric heating. Because of the high efficiency, reliability and flexibility, the choice was made to use solar power combined with a heat exchanger. Once known what time frame is available to reverse the flow direction, the next step is to determine the available solar power during that period, which will be used to determine the reverse flow rates later on. The electrical power generated by solar panels is given by

$$P_{solar} = I \cdot A \cdot \eta \tag{14}$$

Where I is the solar irradiance, A is the area of the solar panels and $\eta$ is the efficiency of the solar panels.

In this report, three scenario's for reversing the flow direction will be tested.

- Scenario 1: The solar power currently generated at the TU campus is used to power the system
- Scenario 2: The system will run at maximum flow capacity (350 $m^3/h$)
- Scenario 3: A selected number of buildings at the TU campus is equipped with solar panels to increase available solar power.

By measuring the area of a selection of flat roofs at the TU campus, using Google Earth satellite images, the solar panel area for scenario 3 will be determined. Literature research will be done to find average values for I and $\eta$. Once all these values are known, equation 14 will be used to compute the available power for scenario's 1 and 3. This power will be used to compute the reverse flow rates later in section 3.4. For scenario 2, the flow rate is already known (max system capacity) and the required power and solar panel area will be computed later in section 3.4.

## 3.3 Analytical thermal front model

To assess the effect of reversing the flow direction, an advection based analytical model was used that simulates the position of the thermal front over time. This section shows all the steps taken to build this model.

### 3.3.1 Baseline simulation setup

To determine the effect of seasonally reversing the flow direction, it's crucial to first establish and verify a baseline simulation of the thermal front and breakthrough time. This model was build step by step. First, a linear model based on advection only was made. Using the production rate $Q$ and an assumed cross-sectional area $A$, the Darcy velocity was calculated using

$$v_d = \frac{Q}{A} \tag{15}$$

The corresponding pore velocity was then computed using

$$v_p = \frac{v_d}{\phi} \tag{16}$$

The location of the thermal front over time can then be calculated using

$$x_{front} = v_p \cdot t \tag{17}$$

and the breakthrough time is computed using

$$t_{breakthrough} = \frac{L}{v_p} \tag{18}$$

This model however is too simplified since it doesn't take into account the thermal storage capacity of the rocks in the reservoir. To account for this, the thermal mobility coefficient $\lambda$ was introduced in the model, which is computed as follows:

$$\lambda = \frac{\phi \rho_f c_f}{\phi \rho_f c_f + \rho_r c_r (1 - \phi)} \tag{19}$$

the new velocity of the cold front is then computed using

$$v_c = v_p \cdot \lambda \tag{20}$$

With this velocity, the position of the thermal front over time can be visualized. This model gives a basic idea of flow in the subsurface, but it uses linear flow whilst in geothermal reservoirs, radial flow is more realistic as the fluid spreads out radially from the wells. Because of this, even with a constant flow rate, the velocity of the thermal front is not constant but decreases over time as the radius of the cold plume increases. The Darcy velocity in radial coordinates is given by

$$v_d = \frac{Q}{2\pi r h} \tag{21}$$

Similar to the linear model, the pore velocity is then calculated using

$$v_p = \frac{v_d}{\phi} = \frac{Q}{2\pi r h \phi} \tag{22}$$

and including the thermal mobility coefficient $\lambda$, the velocity of the cold front becomes

$$v_c = v_p \cdot \lambda = \frac{Q\lambda}{2\pi r h \phi} \tag{23}$$

To compute and visualize the position of the thermal front over time, iterations are done with a predefined timestep to compute the velocity and position of the thermal front over time until the front reaches the production well.

To further improve the model, the net-gross ratio will be added to the model. This ratio between sandstone and shale affects the porosity, rock density and rock thermal heat capacity through the following three equations

$$\phi = ng \cdot \phi_{sst} + (1 - ng) \cdot \phi_{shl} \tag{24}$$

$$\rho_{rock} = ng \cdot \rho_{sst} + (1 - ng) \cdot \rho_{shl} \tag{25}$$

$$c_{rock} = ng \cdot c_{sst} + (1 - ng) \cdot c_{shl} \tag{26}$$

By adding this to the model, the net-gross ratio becomes an input that affects the porosity $\phi$ and thermal mobility coefficient $\lambda$.

To verify the analytical model and find realistic reservoir properties, it will be compared to an established numerical model (Chen, Rongier, Mullins, Voskov, & Daniilidis, 2025) that simulates thermal breakthrough in the Delft geothermal reservoir. The numerical comparison model uses a distribution for the reservoir properties because of the reservoir heterogeneity. The analytical model assumes a homogeneous reservoir. First, a sensitivity analysis will be performed to see how the model responds to input changes for certain parameters.

### 3.3.2 Sensitivity analysis

To do this sensitivity analysis, the Distance-based generalized sensitivity analysis (DGSA) python version from Perzan, Babey, J. Caers, Bargar, & Maher, (2021) was used. In this process, random samples are taken following a uniform distribution for the flow rate, reservoir thickness, well spacing and net-gross ratio. For each sampled set, the breakthrough time then has to be computed. However, doing the iterations over time for each of the 1000 sample sets is a computationally very time-consuming process.

If a plot of the front position over time is not required, the thermal breakthrough time can also be computed directly by solving the integral

$$t_{breakthrough} = \int_{r_{well}}^{r_{reservoir}} \frac{dr}{v_c(r)} = \int_{r_{well}}^{r_{reservoir}} \frac{2\pi r h \phi}{Q\lambda} dr = \frac{2\pi h \phi}{Q\lambda} \int_{r_{well}}^{r_{reservoir}} r dr \tag{27}$$

which yields

$$t_{breakthrough} = \frac{\pi h \phi}{Q\lambda}(r_b^2 - r_w^2) \tag{28}$$

Where $r_b$ and $r_w$ are the radii of thermal breakthrough and the well respectively. Using this equation, the breakthrough time for each sample set was computed. The results are then categorized into 3 clusters. These are used in the DGSA function to perform the sensitivity analysis. This sensitivity analysis was then used to assess which parameters have the largest effects on breakthrough time when changed.

### 3.3.3 Matching the models

To verify the analytical model, the results had to be matched to those from the numerical model used by Chen, Rongier, Mullins, Voskov, & Daniilidis, (2025). The production temperatures from this model and their derivatives were plotted and used to determine the P10, P50 and P90 breakthrough times for this simulation, where the time of breakthrough was defined as the point where the initial linear temperature drop transitions into a steeper temperature drop. The analytical model assumes a homogeneous reservoir where the whole reservoir is used for fluid flow, which is not accurate as heterogeneity in reservoirs means some parts of the reservoir are not suitable for fluid flow. Furthermore, the analytical model ignores a lot of processes that are taking place in real reservoirs. To match the values of the numerical model, an equivalent reservoir thickness has to be determined. By varying this thickness and the n-g ratio, the reservoir properties for the analytical model were determined to match the P10, P50 and P90 breakthrough times.

## 3.4 Computing reverse flow rates

With the known reservoir properties from the baseline model and the previously calculated available solar power $P_{available}$, the available solar power is used to compute the reversed flow rate that can be delivered. To run the geothermal system in reverse, the available solar power must be used to both heat the water and run the pumps in the system. The Power required to heat a mass flow $m$ with a temperature difference $\Delta T$ is given by:

$$P_{heating} = \frac{mc_p\Delta T}{COP} \tag{29}$$

Where m is the mass flow rate, $c_p$ is the specific heat capacity of water, $\Delta T$ is the temperature difference and COP is the coefficient of performance of the heat pump. The power required by the pumps is given by:

$$P_{pump} = \frac{\Delta P \cdot Q}{\eta} \tag{30}$$

where $\Delta P$ is the total pressure difference, Q is the flow rate and $\eta$ is the efficiency of the pump. The pressure difference in a single well is given by

$$dP_{well} = \frac{Q\mu}{2\pi kh} log(\frac{L}{r_w}) \tag{31}$$

where Q is the flow rate, $\mu$ is the viscosity of the fluid, k is the permeability, h is the reservoir thickness, L is the spacing between the wells and $r_w$ is the radius of the well.

The total pressure difference $\Delta P$ is obtained by adding the pressure differences $dP$ in the production and injection well. Adding the power for the heating and the pumps gives the total required electrical power for a given flow rate.

The goal is to find a flow rate for which $P_{pump} + P_{heating} = P_{available}$. To do this, a root-finding method (bisect) in python will be used. This way, the return flow rates for scenario's 1 and 3 will be computed. For scenario 2 the calculation will be reversed and the required solar power (and thus area) to provide max flow rate will be computed.

To calculate the total COP of the reverse flow process, the thermal power delivered back into the geothermal system ($P_{heating} \cdot COP_{heatpump}$) is divided by the power used in this process $P_{heating} + P_{pump}$

### 3.5 Reversing flow direction

To reverse the flow direction, the same base model was used as for the baseline simulation but with some changes. Rather than a continuous flow in one direction, the model has to simulate periodic change in flow direction. To do this, the model uses multiple cycles where each cycle is one year. In each cycle, iterations are first done for normal flow as in the baseline simulation, with the thermal front reaching a certain position (radius). After the determined production time, the iterations are done with a negative velocity, starting from the position that was reached by the thermal front in the production time. This way, the position of the thermal front can be simulated over time until thermal breakthrough occurs. The position of the thermal front for each of the three scenarios will be plotted against the baseline simulation to visualize the effects on breakthrough time.

### 3.6 Effects of well spacing and reservoir thickness

With the baseline and reverse flow simulations completed, some more in depth analysis can be done for the influence of well spacing and reservoir thickness.

Reversing the direction of flow during summer is expected to increase the time until thermal breakthrough, meaning the system can be used for longer. However, this is not always desired. Geothermal systems face several challenges that have to be taken into account in the design phase. One of them is corrosion in the system. Geothermal fluids can cause corrosion in the system, which affects the production equipment (Nogara & Zarrouk, 2018). Furthermore, drilling is expensive so where possible, closer well spacing is preferred. Seasonally reversing the flow direction means that the same lifespan can be achieved with a closer well spacing.

In this section, the effects of reservoir thickness and well spacing on the lifetime extension that flow reversal can offer will be studied. First, a contour plot will be made to visualize the added lifespan of the reservoir as a function of thickness and well-spacing. After this, the goal is to find how much well spacing can be reduced when seasonally reversing the flow direction. To do this, the properties of the P50 reservoir will be used to find the well spacing that results in the P50 lifespan from the baseline simulation. The analytical model from the previous section is used but the well spacing is varied. A range of well-spacings is created, and the breakthrough time is computed for each of these. This way, the breakthrough time will be plotted as a function of the well spacing. The target breakthrough time (P50 baseline breakthrough time) will also be plotted and the intercept point gives the new well-spacing. This will be done for each of the three scenario's.

## 4 Results

### 4.1 Heat and energy demand

Using temperature data from the KNMI weather station near Rotterdam, the average monthly temperatures were computed for the period 2010-2024. The resulting temperatures were combined in a single plot and can be seen in Figure 4 below.

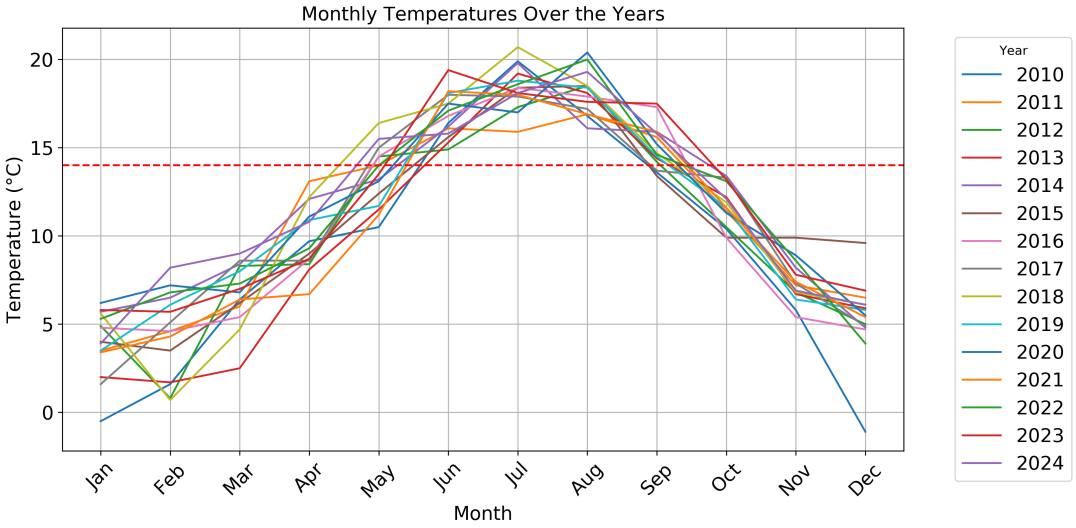


Figure 4: Average monthly temperatures 2010-2024, data from KNMI

The intersection between the temperature plots and the dotted red line in Figure 4 suggests that average temperatures are almost certain to be above 14 degrees for a period of around 3 months from June through August. Figure 5 below further supports that annual heat demand is lowest around weeks 22 (beginning of June) to 35 (end of August). Taking this into account, the remainder of the report will consider the period of three months (June, July, August) as having no heat demand and thus being suitable for reversing the geothermal flow direction.

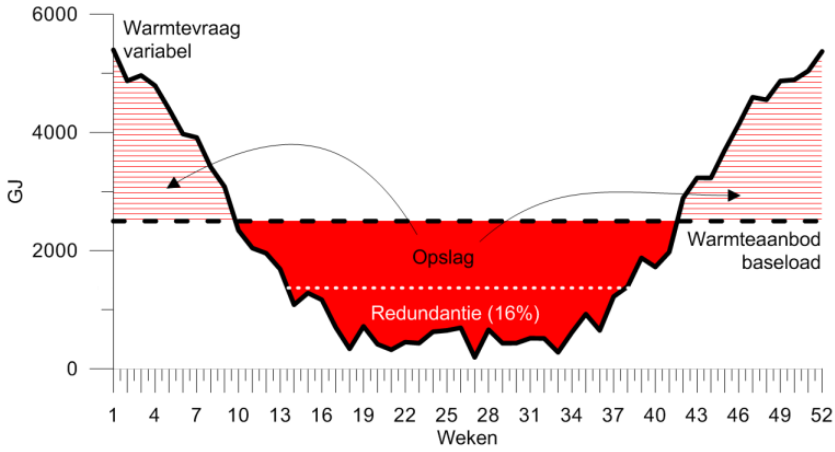


Figure 5: Annual heat demand. From Hartog, Bloemendal, Slingerland, & Van Wijk, (2016)

## 4.2 Available solar energy

The TU Delft campus has a total of 10 000 square metres of solar panels on campus (Delta, 2015). From Wedia, (2022) it was found that the average solar irradiance (24h) during summer in the Netherlands is 239 $w/m^2$. Based on the available information, the efficiency of solar panels is assumed at 20%.
Using this data in equation 14, the available power from the solar panels in scenario 1 is 478kW.

In the second scenario, the reversed injection would run at full capacity for the period of three months. The energy required for this depends on reservoir properties thus this will be computed in section 4.4.

For the third scenario, it was evaluated what power would be available if solar panels were to be installed on a selection of existing buildings and faculties in addition to the existing 10 000 square metres. These buildings and their flat roof area are shown in Table 1.

Table 1: Roof area for limited solar power expansion

| Building | Flat Roof area ($m^2$) |
|---|---|
| CITG (23) | 3500 |
| TNW (22) | 7000 |
| TNO lab (18) | 4000 |
| ME (34) | 3700 |
| EWI (lower part) (36) | 1800 |
| Dream hall (23) | 1800 |
| Already in use | 10000 |
| Total | 31800 |

By installing solar panels on the flat roofs of these 6 buildings, the 31 800 square metres of solar panels will be able to provide 1520kW of electrical power. The results of this section are summarized in the table below.

Table 2: Solar panel area and power per scenario

| Parameter | Scenario 1: Currently available | Scenario 2: Maximum system capacity | Scenario 3: Limited expansion solar power |
|---|---|---|---|
| Area of solar panels ($m^2$) | 10000 | — | 31800 |
| Available solar power ($kW$) | 478 | — | 1520 |

## 4.3 Analytical thermal front model

### 4.3.1 Baseline simulation setup

First, the model using linear flow without thermal storage capacity was made. The parameters used for this can be seen in Table 3 below.

Table 3: Linear baseline simulation properties

| Parameter | Value |
|---|---|
| Flow rate ($m^3/h$) | 320 |
| Porosity (-) | 0.16 |
| Well spacing ($m$) | 1500 |
| Cross-sectional area ($m^2$) | 90000 |

After this, the thermal storage factor $\lambda$ was added to the model. The simulation was then done again using the parameters mentioned above and additionally using the input shown in Table 4.

Table 4: Input parameters thermal storage factor

| Parameter | Value |
|---|---|
| Density water ($kg/m^3$) | 1000 |
| Thermal heat capacity water ($J/kg \cdot K$) | 4186 |
| Density rock matrix ($kg/m^3$) | 2600 |
| Thermal heat capacity rock matrix ($J/kg \cdot K$) | 880 |

The position of the thermal front over time was plotted for both simulations in one graph to show the difference caused by the thermal storage factor $\lambda$. These results can be seen in Figure 6 below.

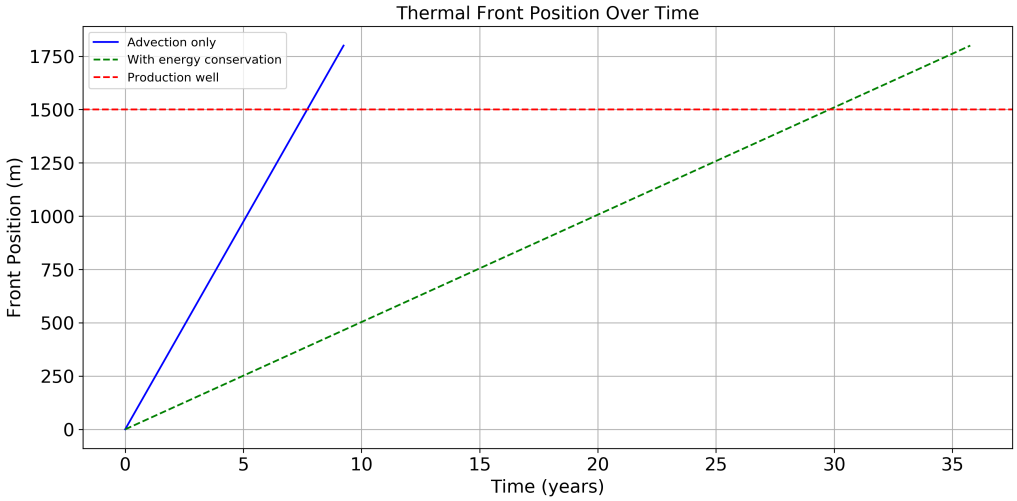


Figure 6: Breakthrough times linear model

The model was then updated to simulate radial flow instead of linear flow. The parameters from above were used and some more were added to simulate the radial flow, these can be seen in Table 5.

Table 5: Radial baseline simulation properties

| Parameter | Value |
|---|---|
| Reservoir thickness (m) | 80 |
| Well radius (m) | 0.1 |
| Radius breakthrough (m) | 1500 |

The simulation was then done with and without the thermal storage factor $\lambda$. The resulting plot of the thermal front position can be seen in Figure 7

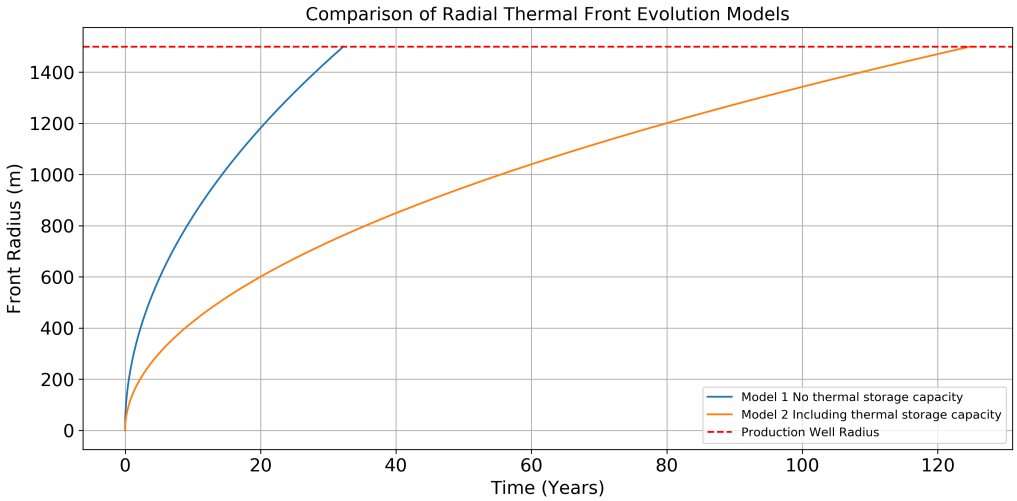


Figure 7: Breakthrough times radial model

To complete the baseline model, the net to gross ratio was integrated where the following values were used for the sandstone and shale properties.

Table 6: Rock properties for net-gross ratio

| Parameter | Value |
|---|---|
| Density sst ($kg/m^3$) | 2600 |
| Thermal heat capacity sst ($J/kg \cdot K$) | 880 |
| Density shale ($kg/m^3$) | 2650 |
| Thermal heat capacity shale ($J/kg \cdot K$) | 850 |
| Porosity sandstone (-) | 0.2 |
| Porosity shale (-) | 0.1 |
| Net-Gross ratio (-) | 0.7 |

The thermal front evolution of this final model can be seen in Figure 8 below.

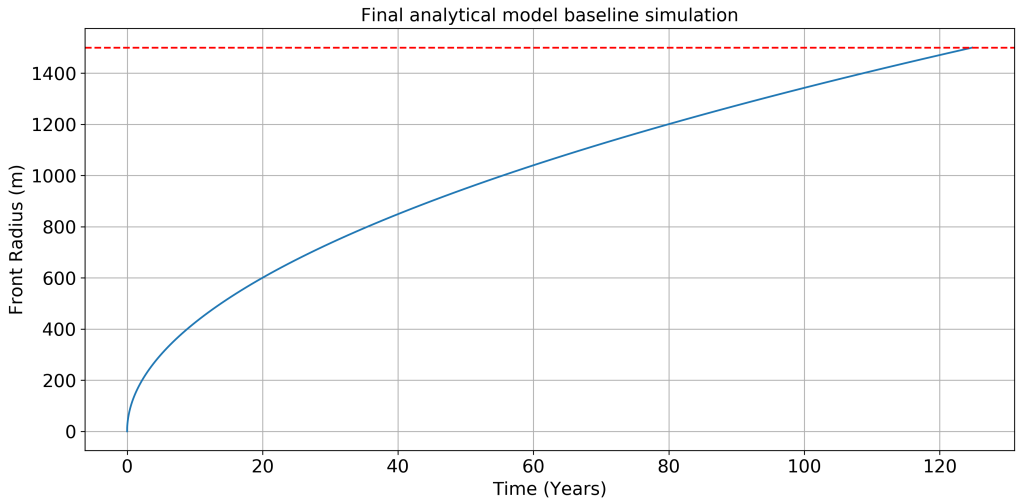


Figure 8: Final analytical model

### 4.3.2 Sensitivity analysis

In the DGSA sensitivity analysis, the response of the model to changes in input was analysed. The sensitivity analysis was done using variations in flow rate ($Q$), reservoir thickness ($h$), well spacing ($r_b$) and net-gross ratio ($ng$) with a uniform spread as shown in the table below.

Table 7: Parameter distribution sensitivity analysis

| Parameter | Value |
|---|---|
| Flow rate ($m^3/s$) | 0.041-0.09 |
| Reservoir thickness (m) | 80-120 |
| Well spacing (m) | 1100-1300 |
| Net-gross ratio (-) | 0.2-0.8 |

The results of the DGSA sensitivity analysis can be seen in Figure 9 below.

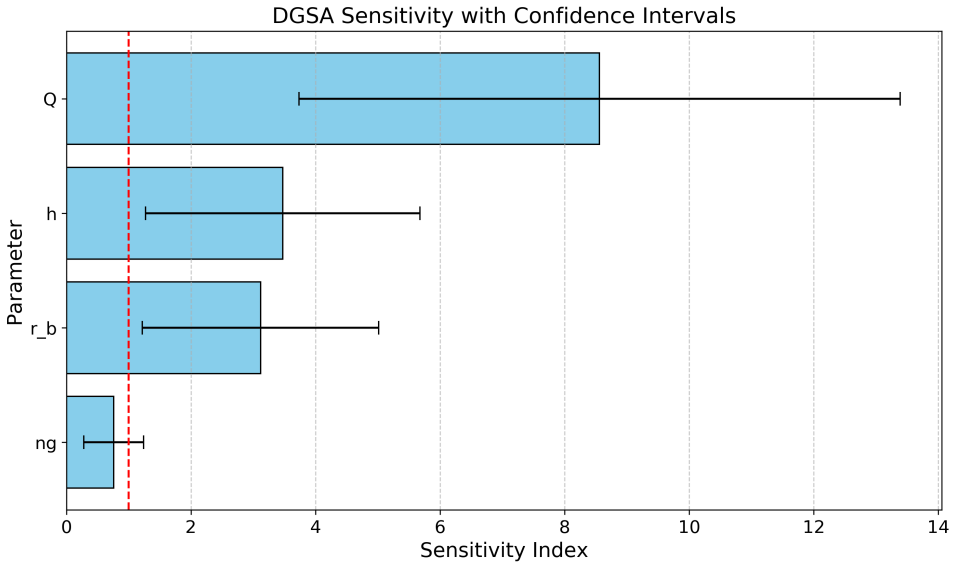


Figure 9: DGSA sensitivity analysis

What stands out in this analysis, is the low sensitivity index for the net-gross ratio. The net-gross ratio directly affects the porosity and one would therefore expect this to greatly affect the pore velocity and thus the breakthrough time. However, the porosity in it's turn also influences the lambda value. To further clarify this relation, a contour plot of porosity and lambda values with the corresponding breakthrough time was made. This can be seen in Figure 10 below.

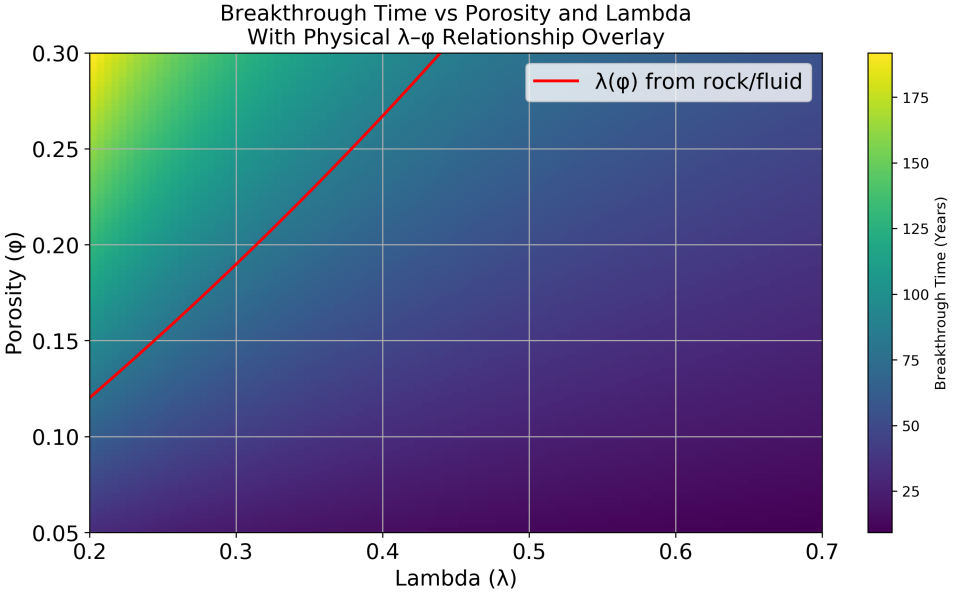


Figure 10: Breakthrough time vs porosity and lambda

In this plot, the relationship between porosity and the corresponding lambda values is shown (red line). One can see that along this line, the breakthrough time barely changes, which explains the low sensitivity index. The reason for this will be analysed in the discussion.

### 4.3.3 Verifying the model

The production temperatures from the numerical model, including the P10, P50 and P90 temperatures can be seen in Figure 11

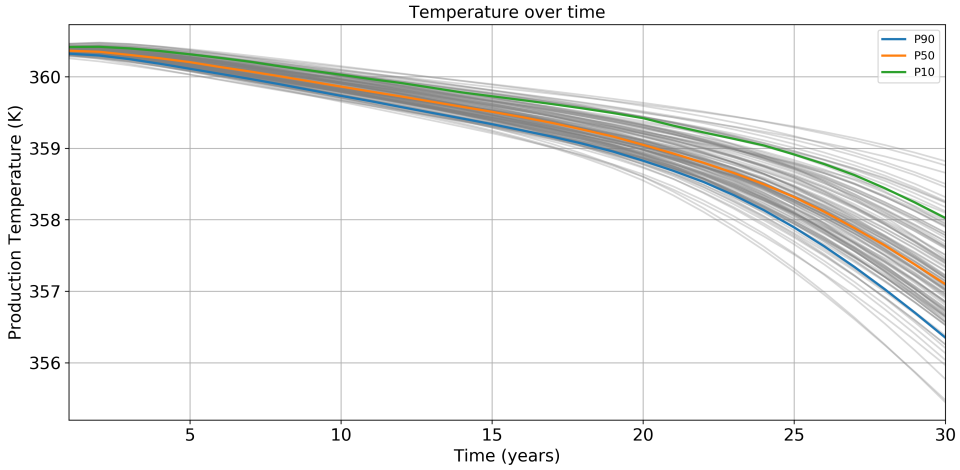


Figure 11: Numerical production temperatures. Data from Chen, Rongier, Mullins, Voskov, & Daniilidis, (2025)

To help determine the breakthrough time, the change in slope (derivative) of the P10, P50 and P90 curves was also computed and can be seen in Figure 12

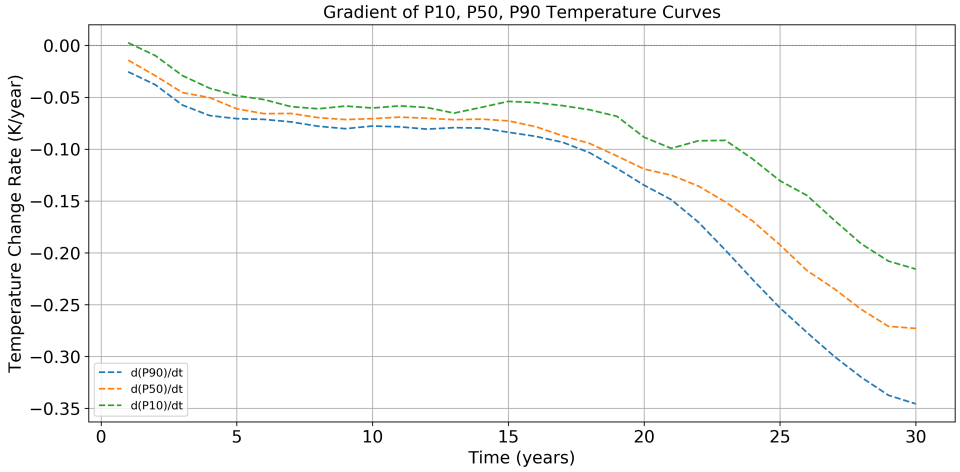


Figure 12: Derivative of numerical production temperatures

Based on this plot, the thermal breakthrough times were determined as follows.

| Temperature curve | Time (years) |
|---|---|
| P10 | 24 |
| P50 | 21 |
| P90 | 18 |

The flow rate and well-spacing from the numerical model were then used to find the equivalent thickness that makes the P50 scenario match the analytical model for a net to gross ratio of 0.5. This turns out to be a thickness of $h_{equivalent} = 28m$. To match the P10 and P90 scenario's, n/g ratios of 0.8 and 0.2 respectively were used and the equivalent thicknesses for these scenario's are 31 and 25 metres. The baseline simulation for the P10, P50 and P90 breakthrough times using these input parameters can be seen in Figure 13 below.

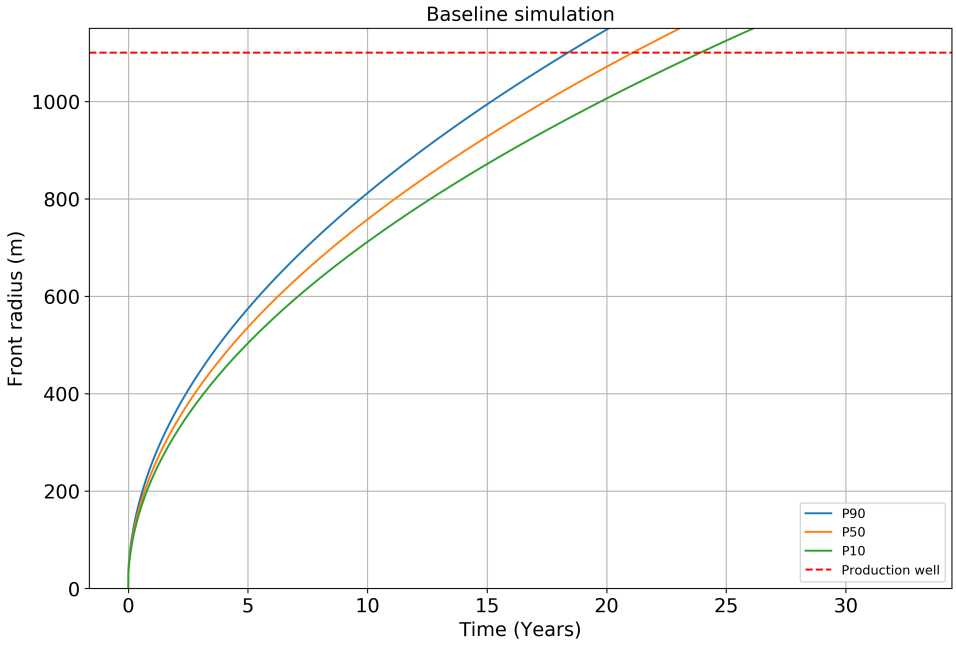


Figure 13: Thermal front baseline simulation

## 4.4 Determine reverse flow rates

With the available solar power and the P50 reservoir properties, the reversed flow rate was calculated, taking into account that both the heating process and the pumps need energy. All used input parameters can be found in the table below.

Table 8: Parameters for flow rate calculations

| Parameter | Scenario 1 |
|---|---|
| Thermal heat capacity water $(J/kg \cdot K)$ | 4186 |
| dT (K) | 30 |
| COP (-) | 3 |
| $\mu_{inj}$ $(Pa \cdot s)$ | 0.000589 |
| $\mu_{prd}$ $(Pa \cdot s)$ | 0.000377 |
| well spacing (m) | 1100 |
| well radius (m) | 0.1 |
| k $(m^2)$ | 9.9e-13 |
| Efficiency pump $\eta$ (-) | 0.5 |
| h (m) | 28 |

Using these parameters together with the available solar power from table 2 in section 4.2, the return flow rates for Scenario 1 and Scenario 3 were computed. These turn out to be 39.996 and 120.744 cubic metres per hour respectively. For scenario 2 (maximum system capacity of 350 $m^3/h$), the calculation was reversed and the required amount of solar energy (and solar panel area) to achieve this flow rate was computed. It turns out that an area of 105 550 square metres is required to provide this flow rate. All results, including the energy used for pumping and heating, the reservoir pressure drop and the reversed flow COP can be seen in Table 9 below.

Table 9: Reverse flow rates, power requirements and COP

| Parameter (P50) | Scenario 1 | Scenario 2 (A=105550) | Scenario 3 |
|---|---|---|---|
| Available solar power (kW) | 478 | 5045.29 | 1520 |
| Return flow rate (kg/s) | 11.11 | 97.22 | 33.54 |
| Return flow rate (mˆ3/h) | 39.996 | 350 | 120.744 |
| dP (Pa) | 573636 | 5017732 | 1730999 |
| dP (bar) | 5.7 | 50.2 | 17.3 |
| Pump power (kW) | 12.75 | 975.65 | 116.07 |
| Heating Power (kW) | 465.25 | 4069.64 | 1403.93 |
| COP reverse flow process (-) | 2.92 | 2.42 | 2.77 |

## 4.5 Geothermal reservoir lifespan

To simulate the effects of periodic flow reversal, the three scenario's from Table 9 (section 4.4) were used and the simulation was done for the P10, P50 and P90 reservoir conditions. The simulations were done using the following parameters.

Table 10: Properties for reversed flow simulation

| Parameter | Value |
|---|---|
| Porosity sandstone (-) | 0.2 |
| Porosity shale (-) | 0.1 |
| Well spacing (m) | 1100 |
| Cyclic production time (months) | 9 |
| Cyclic reversing time (months) | 3 |
| Density water ($kg/m^3$) | 1000 |
| Specific heat capacity water ($J/kg \cdot K$) | 4186 |
| Density sst ($kg/m^3$) | 2600 |
| Specific heat capacity sst ($J/kg \cdot K$) | 880 |
| Density shale ($kg/m^3$) | 2650 |
| Specific heat capacity shale ($J/kg \cdot K$) | 850 |

| Parameter | P10 | P50 | P90 |
|---|---|---|---|
| Reservoir thickness (m) | 31 | 28 | 25 |
| net to gross ratio (-) | 0.8 | 0.5 | 0.2 |

The figures below show the P10, P50 and P90 lifespan for the three different reverse flow rate scenario's against the baseline simulation.

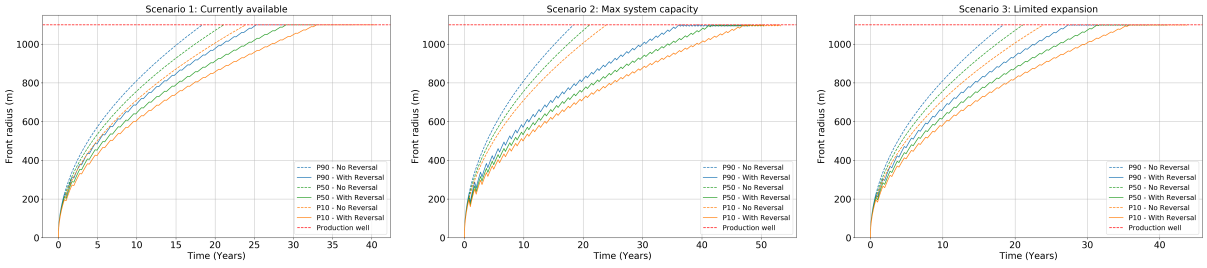


(a) Currently Available (b) Max Capacity (c) Limited Expansion

Figure 14: Reverse flow simulations

## 4.6 Thickness and well spacing effect

Using the reservoir parameters from the P50 baseline simulation, the additional time until breakthrough was visualized as a function of well-spacing and thickness for each of the three scenario's. The results can be seen in Figure 15 below.

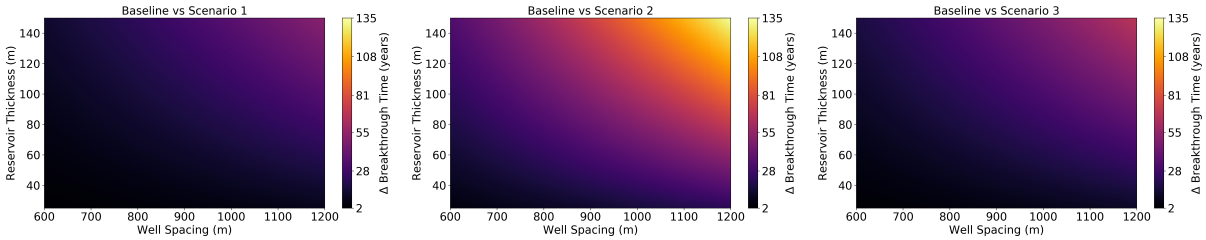


(a) Currently Available (b) Max Capacity (c) Limited Expansion

Figure 15: Added lifetime as function of reservoir thickness and well spacing

To determine how much well spacing can be reduced, the breakthrough time was plotted as a function of the well spacing for the reversed flow simulation. The results of this can be seen in Figure 16.

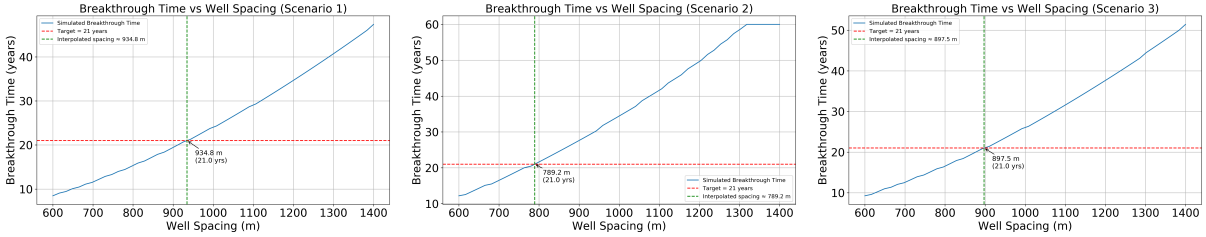


(a) Currently Available (b) Max Capacity (c) Limited Expansion

Figure 16: Reduced well spacings with baseline simulation lifetime

# 5 Discussion

## 5.1 Heat and energy demand

The period of three months in which temperatures are high enough that significant heating is not required offers a good potential for reversing flow and recharging the geothermal system. This is important to know because it shows whether there is an available time frame for reversing the flow direction. What is important to keep in mind though, is that this reversal of flow means that no hot water will be produced by the system during this period which could be problematic if the geothermal system heat is also used for other purposes than just district heating.

## 5.2 Available energy

To heat the water in the reverse flow process, solar power will be used. From the results, it can be seen that the current available power at the TU campus during these three months is 478kW, which is relatively limited as will be discussed later. However, by expanding the TU's solar panel area using some of the flat roof buildings on campus, the area can be more than tripled to 31 800 square metres. This would increase the available electrical power to 1520kW. Important to note here is that these calculations are based on an average 24h solar irradiance of 239 $w/m^2$ whilst in reality this power is not spread uniformly throughout the day (0 at night, upwards of 800 $w/m^2$ during sunny daytime). If the goal is indeed to solely use the campus solar power directly, additional research is required to temporarily store either the excess power or heated water during daytime to deliver the same constant flowrate throughout the night. For this report, the average 24h irradiance was assumed to obtain a constant power and flow rate throughout the whole period.

## 5.3 Analytical thermal front model

In the results from the baseline simulation setup, the results for every step of the model are shown. Using typical reservoir properties, the first simulations (using linear flow) show breakthrough times of 7.5 (without thermal mobility coefficient) and 30 (with thermal mobility coefficient) years. In geothermal wells, flow is radial rather than linear thus the model was adapted and with the same properties had breakthrough times of 31 and 123 years respectively. This difference can be explained because the

velocity in radial flow decreases with an increasing radius thus as the front spreads out further, it slows down resulting in a longer breakthrough time.

In the sensitivity analysis, the large effect of the flow rate is not surprising as the uniform spread used is quite large and it directly impacts the darcy velocity and thus breakthrough time. What does stand out is the limited effect of the ng ratio. Because of this, the additional contour plot in section 4.3.2 was made to show the relationship between porosity (determined by n-g ratio), lambda (influenced by porosity) and breakthrough time. Along the line with possible porosity-lambda values, the breakthrough time barely varies, which explains the low sensitivity index. The explanation for this lies in equation 28. In Figure 10, one can see the relation between porosity and lambda is nearly linear. In equation 28, porosity $\phi$ is in the enumerator, whilst $\lambda$ is in the denominator, meaning that any proportional changes will pretty much cancel each other out. This explains the little variation in breakthrough time with a changing n-g ratio.

A large limitation of the analytical model is that it assumes a homogeneous reservoir that is in it's entirety available for flow and heat storage. In real reservoirs, impermeable reservoir sections and preferred flow paths result in different flow behavior. The breakthrough times of the baseline simulation seem quite long for the reservoir parameters used. To verify that the velocity based model is correct, the breakthrough time was also calculated based on the volume required to fill the pores between the wells and the set flow rate. The result was the same and can be seen in appendix A. The thermal mobility coefficient plays a large role here. Without the thermal mobility coefficient, the breakthrough time (purely flow based) is around 32 years, which is much closer to what one would expect. The thermal mobility coefficient with values around 0.25 delays the advance of the thermal front. The large impact of this is likely because the effect is overestimated. The model now assumes that all heat stored in the rocks is available for production. In real reservoirs, not all the rock heat is used to delay the advance of the thermal front and some heat is likely to stay behind due to other processes such as conduction that are not part of this analytical model. The determined equivalent thicknesses seem to be quite small compared to the actual reservoir thickness but this is likely due to the before mentioned facts that the whole reservoir is assumed to be suitable for fluid flow and that the effect of the thermal mobility coefficient is overestimated. To make the model more realistic, additional research could be done to introduce a coefficient that accounts for impermeable reservoir parts or better takes into account the other processes affecting the temperature evolution in the reservoir. For this report, knowing the equivalent thickness is crucial to match the breakthrough times from the numerical model and provide a reliable reversed flow simulation later on.

## 5.4 Determine reverse flow rates

From the results, the reverse flow rates for each of the three scenarios are known. As seen in Table 9, the return flow rate and thus the amount of recharge in the geothermal system does not scale linearly with the available solar power. This non-linearity is due to the behavior of the system's coefficient of performance (COP). The COP decreases as the flow rate increases. The explanation for this lies in equations 30 and 31. Here one can see that the pumping power depends on the flow rate in two ways: directly through the flow term $Q$ and indirectly through the pressure drop $\Delta P$, which also increases with an increasing flow rate. Because pumping power scales with the square of flow rate, a larger fraction of the available power is consumed by the pumps for higher flow rates thus the overall COP decreases. This is something to keep in mind when determining the targeted reversed flow rate, as the (energy) costs have to be weighted against the gains in reservoir lifetime. Furthermore, the area of solar panels required to run the system at full capacity was determined at 105 550 square metres. Whilst this is a very large area, the TU Delft campus has a total flat roof area of over 170 000 square metres (TU Delft, 2016). Making it theoretically possible to generate all the power on campus.

## 5.5 Geothermal reservoir lifespan

From the results, one can see that with the power currently available, the geothermal reservoir lifetime can be extended by about 7 years (133% of original lifetime) when seasonally reversing the flow direction. With limited expansion this could increase to 11 years (152% of original lifetime) and if the system were to be used at full capacity this could be as much as 21 years (200% of original lifetime). There is also a notable difference between the P10, P50 and P90 reservoir properties, where in each scenario the P10

lifetime increases more than the P50 and P90 lifetimes. This is something that will be discussed in section 5.6 below. Important to note here is that the reverse simulation is compared to a baseline simulation that produces for 12 months a year.

### 5.6 Thickness and Well spacing effect

To further analyze the effect of reservoir properties and the difference in lifetime extension mentioned above, the contour plots in Figure 15 were made. From the contour plots, it shows that for thicker reservoirs, the well spacing has a stronger effect on the extended time until breakthrough and for a constant well-spacing, thicker reservoirs have a larger absolute lifetime extension. This is because reversed flow rates reduce the effective velocity of the thermal front over time. Because the time to thermal breakthrough is proportional to thickness (as shown in equation 28), a larger thickness results in a greater absolute difference even though the relative difference might be the same. This explains why the previous section found that the lifetime in the thicker P10 reservoir increases more than in the P50 and P90 reservoirs. It was also found that when targeting the same 21 year lifespan from the P50 baseline simulation, the well spacing in this case could be reduced from the original 1100 metres to 934.8 metres (15.0% reduction) for scenario 1, down to 897.5 (22.6% reduction) and even 789.2 metres (28.3% reduction) for scenario's 3 and 2 respectively. This shows that periodically reversing the flow direction allows for significantly closer well spacing which could be an important consideration for geothermal projects that need to have a certain lifetime whilst having to limit initial costs or only having limited space available. Furthermore, with buildings becoming more energy efficient and cooling demand expected to increase towards the future, it's not unlikely that at some point in the future, required production and return flow rates are equal. For future studies, determining the required well-spacing to cover the time until these rates match would be very useful for new geothermal projects.

## 6 Conclusion

The purpose of this report was to investigate whether excess energy during summer could be used to reverse the flow direction in a geothermal reservoir by extracting water from the cold well, heating this at the surface and re-injecting it in the hot well. Using an analytical model, the position of the thermal front was simulated and it was determined how much this process could extend the time until thermal breakthrough. In this process, the effects of properties such as thickness and geothermal well spacing were also analysed.

It was found that during the summer months of June, July and August, central heating systems are likely to be turned off and this period could be used to reverse the flow direction. With the 10 000 square metres of solar panels currently available at the TU Delft campus, a limited reversed flow rate of 39.996 $m^3/h$ (11.43% of the maximum system capacity) could be delivered which could extend the system's lifetime by approximately 7 years from the 21 year baseline simulation. By expanding the solar power system on campus using a selection of buildings, 31 800 square metres of solar panels would be able to deliver enough power for a reversed flow rate of 120.744 $m^3/h$ (34.50% of the maximum system capacity). This could extend the lifetime of the system by around 11 years. To run the system at full capacity, 105 550 square metres of solar panels would be required and this could extent the time until thermal breakthrough by 21 years. The absolute effect of reversing the flow direction was found to be greater in reservoirs with a larger thickness. In the simulated Delft reservoir, the well spacing could be reduced from the original 1100 metres down to 934.8 metres (currently available power), 789.2 metres (maximum capacity) or 897.5 metres (limited expansion) whilst keeping the same 21 years breakthrough time from the baseline simulation. It can be concluded that using excess energy in summer to reverse the flow direction in geothermal systems can offer several opportunities to improve the system's performance. Either by extending the time until thermal breakthrough, or by allowing a closer well spacing to limit initial costs.

This research has several limitations and uncertainties. First, it was assumed that all the solar power available is available to heat water from the geothermal system, which is not realistic, as the buildings on campus also need to be powered. Furthermore, the analytical model makes some simplifications that introduce uncertainties. The model assumes a homogeneous reservoir where heat only transports through convection, with a sharp thermal front. Conduction, dispersion and recharge from confining layers are not part of this model. By verifying the baseline simulation with a numerical model and using

an equivalent thickness this was addressed as much as possible but the assumed radial symmetry still causes a degree of uncertainty in the results.

For future work, it would be recommended to run the reversed flow simulation in an enhanced reservoir model that includes reservoir heterogeneity and other forms of heat transport like conduction and dispersion to get a better idea of how heat moves under reversed flow conditions. Furthermore, a comparison with other heat storage systems, such as HT-ATES would be recommended to compare the feasibility of the various systems.

# References


Agemar, T., Weber, J., & Schulz, R. (2014). Deep geothermal energy production in Germany. *Energies*, 7(7), 4397–4416. https://doi.org/10.3390/en7074397

Bloemendal, M., Vardon, P., Medema, A., Snelleman, S., Marif, K., Beernink, S., & Van Oort, T. (2020). HT-ATES at the TU Delft campus. Retrieved from https://www.warmingup.info/documenten/window-fase-1---a1---verkenning-hto-tud---feasibilityht_ates_tudelft.pdf

Chen, Y., Rongier, G., Mullins, J., Voskov, D., & Daniilidis, A. (2025). Coupled numerical and analytical simulation on the Delft Campus geothermal well. In *Proceedings of the Stanford Geothermal Workshop*. Retrieved from https://pangea.stanford.edu/ERE/pdf/IGAstandard/SGW/2025/Chen1.pdf

Delta. (2015, July 6). TU Delft installs 10,000 $m^2$ solar panels on campus. Retrieved June 5, 2025, from Delta website: https://delta.tudelft.nl/article/tu-delft-installs-10000-m2-solar-panels-campus-clone

Eurostat. (2024, February 27). Renewable energy for heating & cooling up to 25% in 2022. Retrieved May 27, 2025, from @EU_Eurostat website: https://ec.europa.eu/eurostat/web/products-eurostat-news/w/ddn-20240227-2?utm_source=chatgpt.com

Fadel, M., Reinecker, J., Bruss, D., & Moeck, I. (2022). Causes of a premature thermal breakthrough of a hydrothermal project in Germany. https://www-sciencedirect-com.tudelft.idm.oclc.org/science/article/pii/S0375650522001699?utm_source=chatgpt.com

Hartog, N., Bloemendal, M., Slingerland, E., & Van Wijk, A. (2016). Duurzame warmte gaat ondergronds. Retrieved from https://api.kwrwater.nl/uploads/2017/02/Duurzame-warmte-gaat-ondergronds.-Warmteopslag-heeft-meerwaarde-voor-warmtenetten-Hartog-Bloemendal-Slingerland-van-Wijk-KWR-Greenvis-(2016).pdf

Nogara, J., & Zarrouk, S. J. (2018). Corrosion in geothermal environment: Part 1: Fluids and their impact. *Renewable and Sustainable Energy Reviews*, 82, 1333–1346. https://doi.org/10.1016/j.rser.2017.06.098

Nurmi, P. A. (2021, May 7). Preliminary evaluation of the Estonian geoenergy potential and overview of available technologies. Retrieved from https://www.researchgate.net/publication/352197150_Preliminary_evaluation_of_the_Estonian_geoenergy_potential_and_overview_of_available_technologies_expert_opinion_for_using_those_technologies_in_the_Estonian_geological_conditions_suggestions_for_poss

Perzan, Z., Babey, T., Caers, J., Bargar, J. R., & Maher, K. (2021). Local and global sensitivity analysis of a reactive transport model simulating floodplain redox cycling. *Water Resources Research*, 57(12). https://doi.org/10.1029/2021wr029723

TU Delft. (2016). A roof that changes colour with the season. Retrieved June 5, 2025, from TU Delft website: https://www.tudelft.nl/sustainability/campus-projects/groene-daken

Wang, L., Li, Y., Zhao, G., Chen, N., & Xu, Y. (2019). Experimental investigation of flow characteristics in porous media at low Reynolds numbers ($Re \to 0$) under different constant hydraulic heads. *Water*, 11(11), 2317. https://doi.org/10.3390/w11112317

Wedia. (2022, September). 2022 was the sunniest summer the Netherlands has ever seen. Retrieved from IamExpat website: https://www.iamexpat.nl/lifestyle/lifestyle-news/2022-was-sunniest-summer-netherlands-has-ever-seen

# Appendix

## A Hand written breakthrough calculation

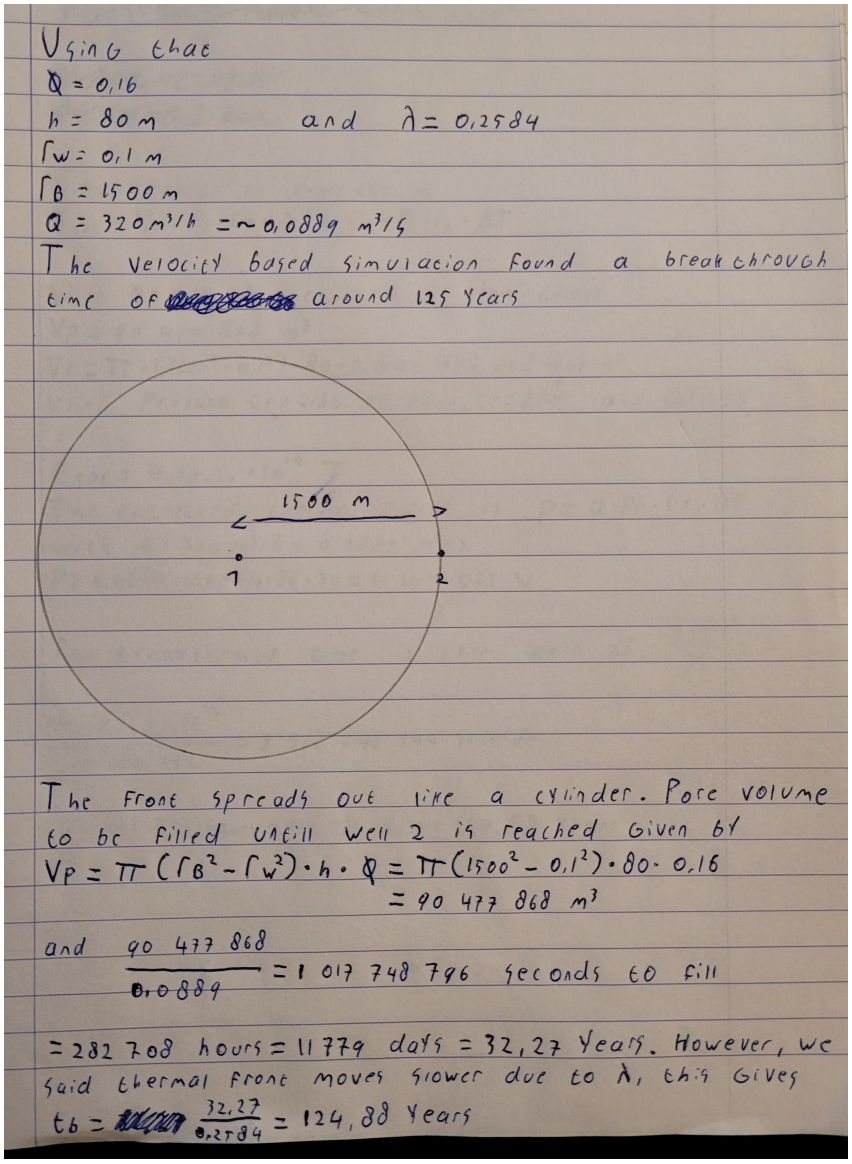


Figure A.1: Volume based breakthrough calculation

# B Full size version of sub-figures

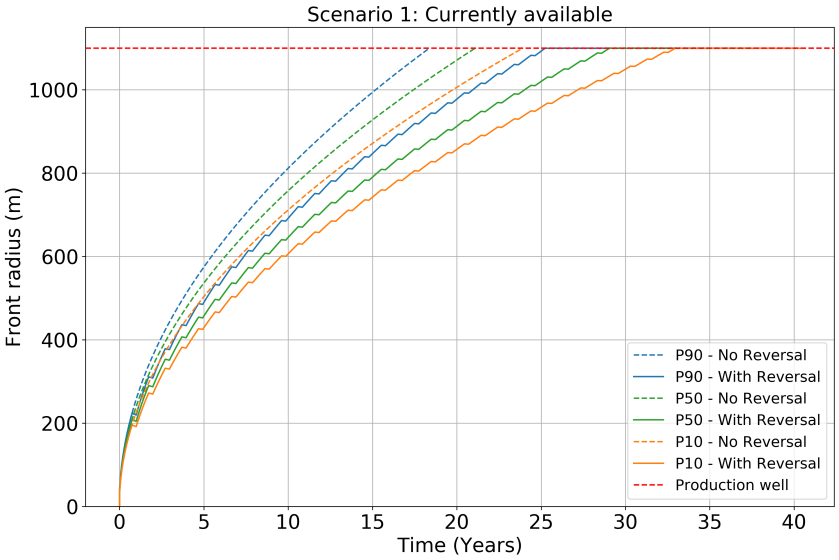


Figure B.1: Reverse flow scenario 1, enlarged figure 14a

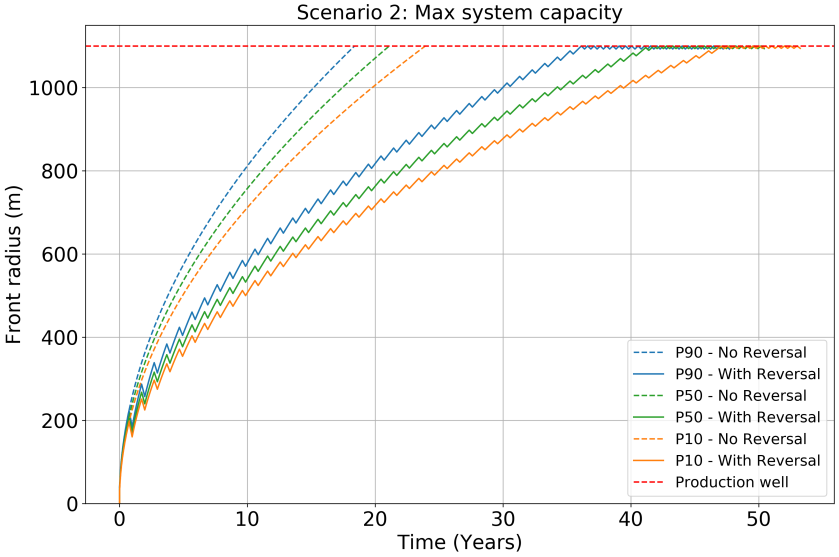


Figure B.2: Reverse flow scenario 2, enlarged figure 14b

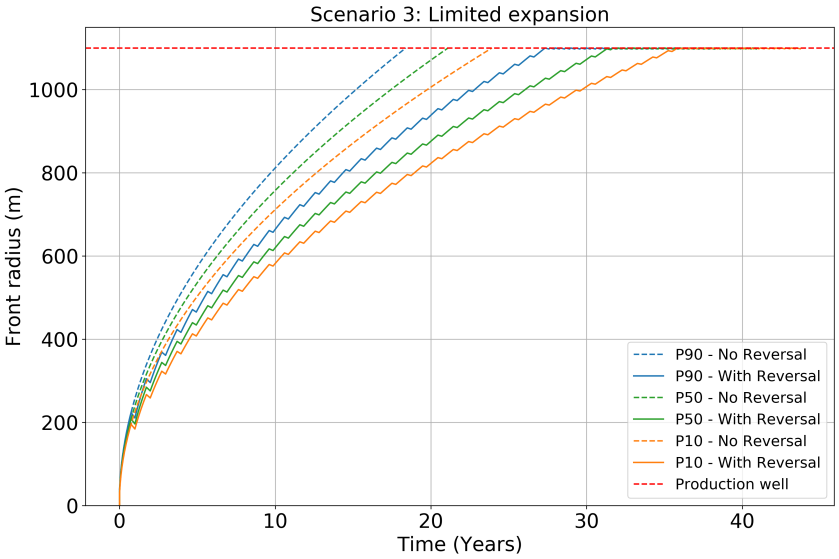


Figure B.3: Reverse flow scenario 3, enlarged figure 14c

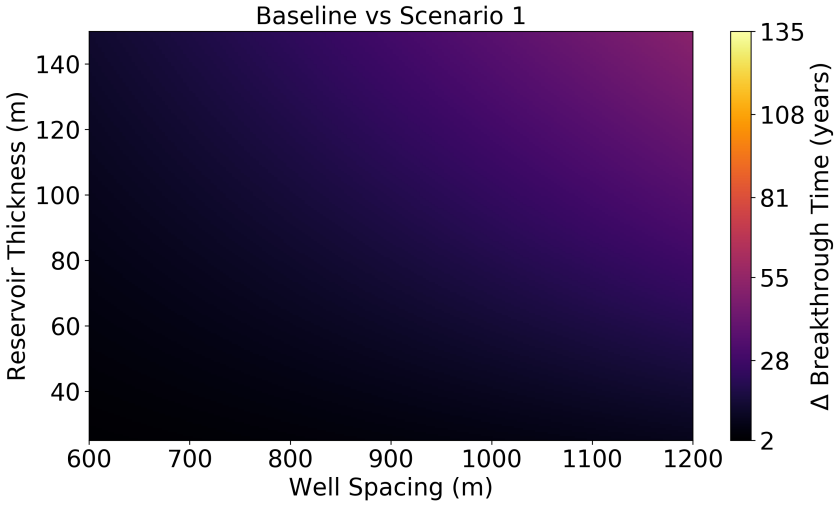


Figure B.4: Thickness and well spacing contour plot scenario 1, enlarged figure 15a

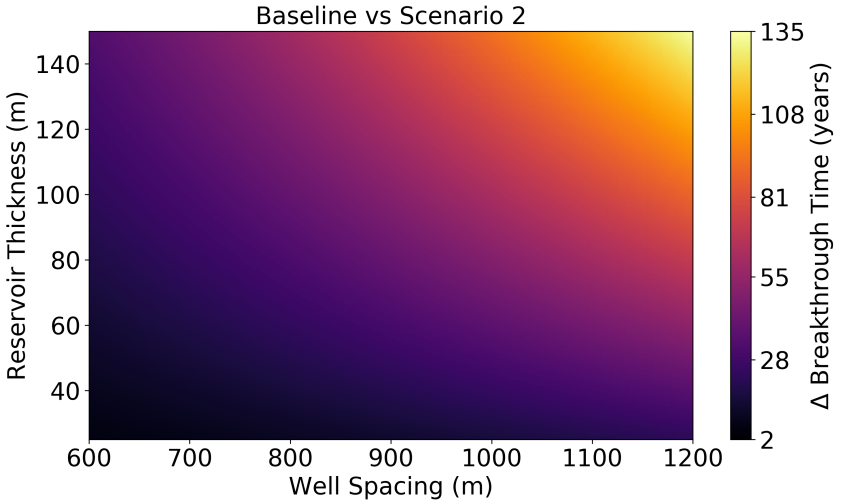


Figure B.5: Thickness and well spacing contour plot scenario 2, enlarged figure 15b

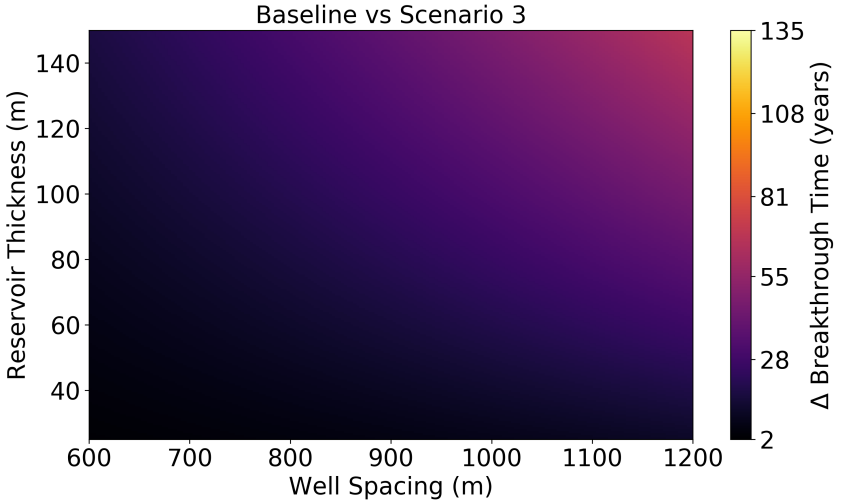


Figure B.6: Thickness and well spacing contour plot scenario 3, enlarged figure 15c

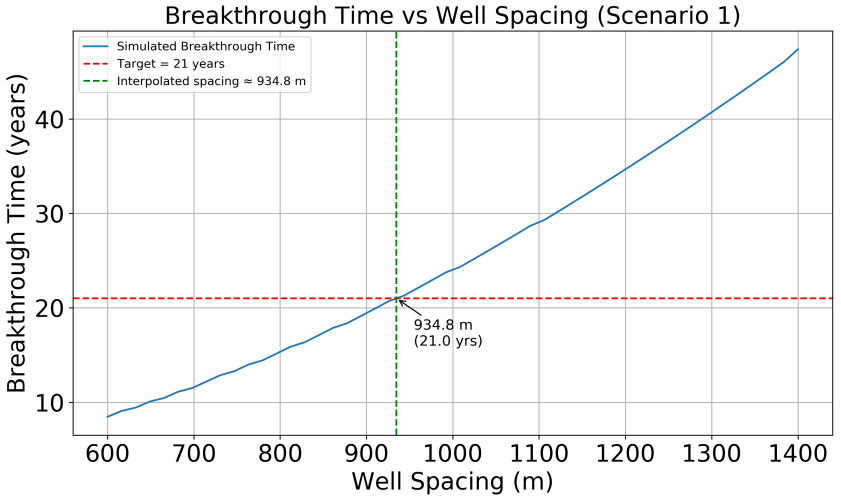


Figure B.7: Reduced well spacing, enlarged figure 16a

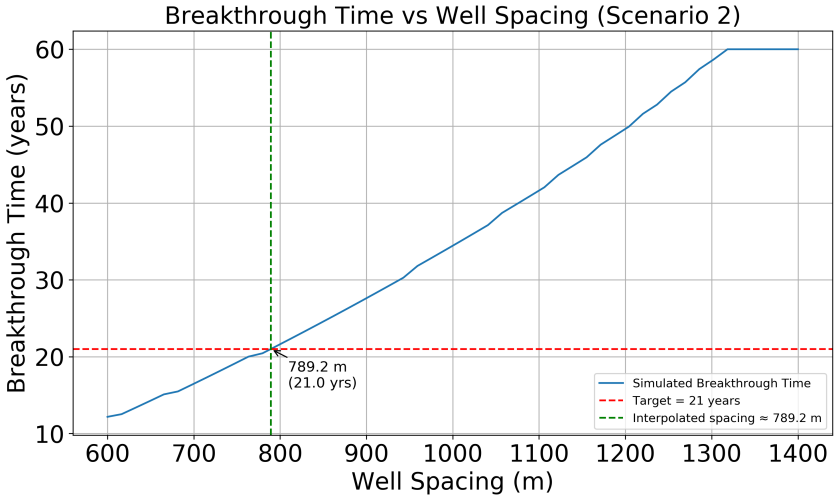


Figure B.8: Reduced well spacing scenario 2, enlarged figure 16b

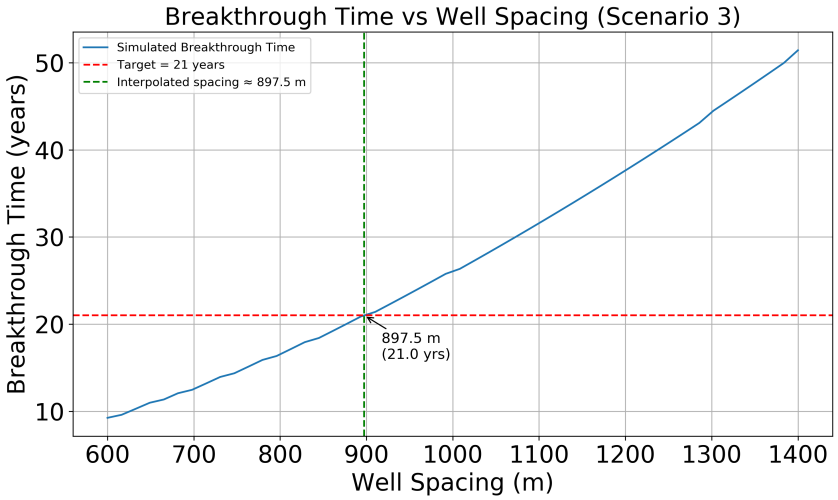


Figure B.9: Reduced well spacing scenario 3, enlarged figure 16c